THE JOURNAL OF PHYSICAL CHEMISTRY A

Article

pubs.acs.org/JPCA

Nature of Hydrogen Bonds and S···S Interactions in the L-Cystine Crystal

Anaid G. Flores-Huerta,[†] Alexandre Tkatchenko,[‡] and Marcelo Galván*[,†]

[†]Departamento de Química, Área de Fisicoquímica Teórica, Universidad Autónoma Metropolitana-Iztapalapa, Av. San Rafael Atlixco 186, Col. Vicentina CP 09340, México, D.F., Mexico

[‡]Fritz-Haber-Institut der Max-Planck-Gesellschaft, Faradayweg 4-6, 14195 Berlin, Germany

ABSTRACT: The intermolecular interactions that govern the stability of the L-cystine crystal were studied. This task is accomplished by using density-functional theory (DFT) with the generalized-gradient approximation (GGA) and including many-body dispersion (MBD) interactions. The strengths of the different interactions within the molecular crystal were obtained by a decomposition of the total interaction energy in two-, three-, and four-body contributions. It was determined that most of the hydrogen bonds formed within the crystal are strong (13, 15, and 19 kcal/mol) and the van der Waals nature of the S···S interaction is fully confirmed. Also, the presence of strong repulsive three-body contributions is determined. The results obtained support the idea of designing crystal growth inhibitors for this system in such a way that, when inserted in the crystal, they maintain the disulfide bridge environment but its capacity of generate hydrogen-bond networks is removed.

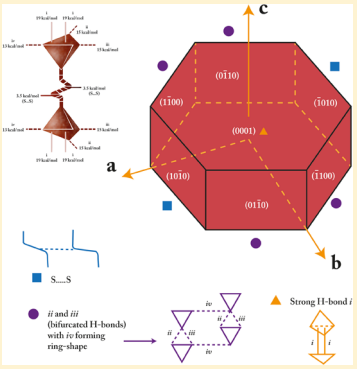

INTRODUCTION

The overproduction of L-cystine causes the formation of crystals that are deposited in the kidneys, eyes, liver, muscles, pancreas, brain, and white blood cells in the human body.[1] Such excess is due to a defective reabsorption of filtered cystine and its low solubility produces the formation of crystals that aggregate into stones, often with centimeter dimensions; the corresponding disease is called cystinosis.[2] Current treatments of cystinosis are highly expensive and their side effects have not yet been fully tackled. The search for new strategies to treat the disease involves identifying molecules that inhibit the L-cystine crystal growth, such as that proposed by Rimer et al., in 2010.[3] Their study found the molecule L-cystine dimethyl ester (L-CDME) reduces the binding of L-cystine molecules and indicated that a key starting point in the design of suitable molecules, as candidates to new treatments, is to have a quantitative description of the main stabilizing forces responsible for the crystal structure and the recognition pattern involved in the growth process.

The L-cystine molecule is formed by two cysteine molecules linked by a disulfide bridge rather than by a peptide bond. The crystal of this dipeptide exhibits polymorphism with tetragonal and hexagonal phases; it crystallizes, *in vitro* at physiological pH, as hexagonal plates with large (001) basal surfaces that can achieve widths of 400 mm and are bounded by six equivalent (100) faces. The hexagonal crystal of L-cystine was first analyzed by Oughton and Harrison[4] in 1959; they established that the unit cell of the crystal has six molecules organized along the C axis forming helical structures; the molecular units exhibit intermolecular N−H···O hydrogen bonds along the C axis (a sort of head-to-tail interaction) and between adjacent helices in the AB (001) plane (Figure 1); also, they suggested

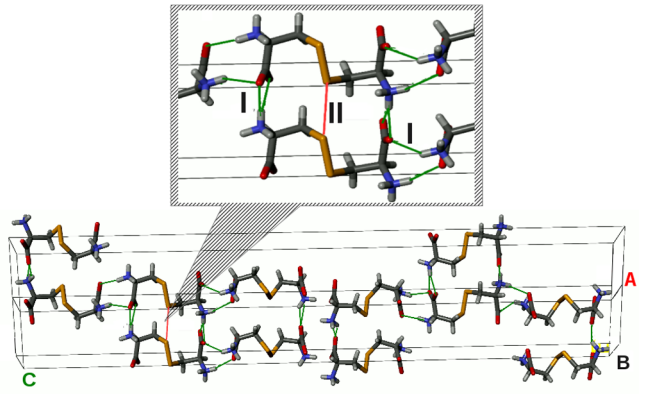

Figure 1. Crystal structure of L-cystine. Two adjacent unit cells along the A direction are displayed. Each unit cell contains six L-cystine molecules in the zwitterionic form. In the zone marked by I the N−H···O hydrogen bonds are explicitly indicated; in the area marked by II the S···S interaction is shown.

the presence of intermolecular S···S interactions normal to the (100) planes because the structure exhibits sulfur atoms in adjacent disulfide bridges separated by a distance much shorter than the sum of van der Waals radii (3.7 Å); later on, Dahaoui et al.[5] by a detailed analysis of the experimental electron density of L-cystine crystal at 110 K, indicate that such interaction could be of van der Waals type. Since the early crystal structure determination in 1959, it was realized that L-cystine crystallize

Received: March 29, 2016
Revised: May 20, 2016
Published: June 1, 2016

DOI: 10.1021/acs.jpca.6b03167
J. Phys. Chem. A 2016, 120, 4223−4230

in a zwitterionic form and the stability of the crystal and low solubility has been related to the hydrogen-bond networks formed within the solid. Indeed, the pattern of intramolecular hydrogen bonds determined for isolated L-cystine conformers by Roux et al.[6] is lost in the crystal structure where the packing effects favor the formation of the interaction network mentioned above.

One of the main structural characteristics of zwitterionic amino-acid crystals is the head-to-tail chains linked via the N−H···O hydrogen bonds between the charged $-COO^-$ and $-NH_3^+$ terminal groups.[7] A key difference between L-cystine and amino acids or standard dipeptides is that each molecule has four terminal groups to form intramolecular hydrogen bonds, two carboxylic and two amino groups; this gives rise to a complex pattern of hydrogen bonds in the crystal. In addition to this interaction network, the L-cystine crystal has S···S close contacts (Figure 1). As has been pointed out, the hydrogen-bond networks present in the L-cystine crystal are of two types: chains of head-to-tail interactions and ring-shape conformation sequences.[8] These features of the crystal were clearly described by Moggach et al.[9] as hydrogen-bond chains along the C axis (Figure 2.1) and the ring-shape conformations (Figure 2.3). Also, it is noteworthy that the S···S interactions are able to form chains in a plane perpendicular to the C axis.

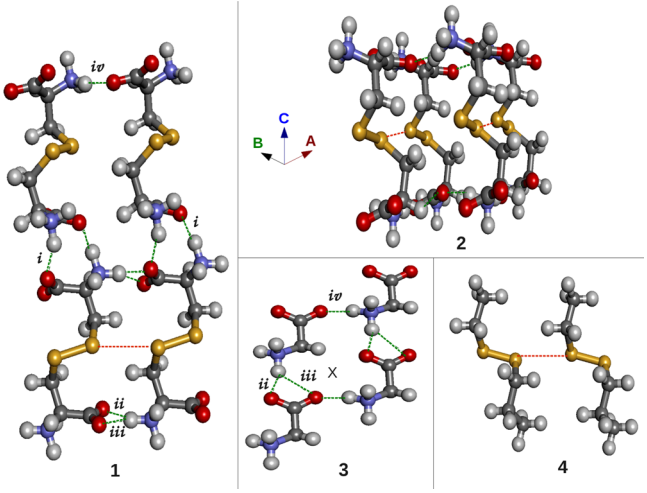

Figure 2. Two tetramers A and B, panels 1 and 2, respectively, extracted from the crystal structure of L-cystine. The hydrogen bonds are identified by the green dotted line, and the S···S interaction is identified with an orange dotted line. The lattice axes are represented with arrows, A axis in red, C axis in blue, and B axis in green. In panel 3 the symbol X indicates a perpendicular view of the cluster B, which shows the ring structure of hydrogen bonds contained in this cluster. Panel 4 displays a structure of two modified L-cystine molecules; this structure was built by using the geometry of the S···S interaction moiety as that of the clusters A or B, but the capping is done with methyl groups to avoid hydrogen-bond formation. The hydrogen bonds are identified by the numbers *i*, *ii*, *iii*, or *iv*.

The remarkable strength of the hydrogen bonds involved in the interaction networks of zwitterionic amino acid crystals has been determined recently for five prototypical amino acid molecular crystals: α-glycine, γ-glycine, L-alanine, DL-serine, and glycylglycine.[10] In that work, a combined experimental and computational study of Young's modulus is performed; one of the main findings is that Young's modulus is strongly facet-dependent and for some particular directions is remarkably high contradicting the common assumption of "softness"of molecular crystals. This unusual stiffness is related to the underlying hydrogen-bonding network and its orientation with respect to each facet. Also, there is evidence that alanine and glycine crystals have very strong N−H···O hydrogen bonds and a large binding energy.[11] As concerns the S···S interaction, it has been suggested that its magnitude is roughly 2 kcal/mol.[12]

Accordingly, the main goal of this work is to evaluate and analyze the intermolecular interactions responsible for the stability of L-cystine crystal including cooperative effects up to four-body contributions. As it has been found that many-body contributions are essential for modeling supramolecular systems, and to describe the stability of molecular crystals,[13,14] this work employed DFT methodologies that include density-dependent nonadditive dispersion methods: the TS[15,16] and MBD[17] methods. In particular, the MBD method takes account of the electrodynamic response (self-consistent modification of the molecular polarizability due to the crystal field), and many-body energy effects, including and beyond the Axilrod−Teller three-body term.[18] The MBD method has proven to be successful in determining molecular binding energies as compared to those obtained by the CCSD(T) method and lattice energies of molecular crystals as compared to several experimental values; it also yields an unprecedented accuracy of 1% in the description of the structures of molecular crystal polymorphs and of 0.2 kcal/mol in their relative energies. In the case of the *b* lattice parameter in β-Gly crystal, where the glycine sheets are bound by bifurcated N−H···O bonds, PBE overestimates by 5%; the PBE-TS method reduces this overestimation to 1% and PBE-MBD yields excellent agreement with experiment.[19]

As the objective is to evaluate the interactions within the solid structure, we consider representative clusters taken out from the crystal structure to study the cooperative effects in ring-shape conformations and head-to-tail chains. The analysis is done by a standard intermolecular many-body expansion[20] that allows us to extract systematically two-body, three-body, and four-body contributions to the total intermolecular interaction energy. By using this procedure, one is able to establish, with detail, the relative weights of the interactions within the crystal, and quantify the many-body effects; in addition, an estimation of the dispersive S···S interaction is obtained.

■ ENERGY DECOMPOSITION

The analysis of the two-body, three-body, and four-body contributions is based on a standard intermolecular many-body expansion,[20]

$$\Delta E_{\text{int}} = E_{\text{tot}} - \sum_{i}^{m} E_i \tag{1}$$

where ΔE_{int} is the interaction energy, E_i, is the energy of an isolated molecule, and E_{tot} is the energy expressed as a sum of one-body, two-body, three-body, four-body, etc., contributions of the whole system:

$$E_{\text{tot}} = E_1 + E_2 + E_3 + E_4 + \ldots \tag{2}$$

With this notation the one-body term, E_1, corresponds to the sum in the right-hand side of eq 1. The analysis is exemplified for a tetramer as follows: the two-body term is

DOI: 10.1021/acs.jpca.6b03167
J. Phys. Chem. A 2016, 120, 4223−4230

$$E_2(abcd) = \sum_{a<b} \epsilon_{ab} = \sum_{a<b} [E(ab) - (E_a + E_b)]$$
$$= \sum_{a<b} [E_{ab} - E_1(ab)] \quad (3)$$

where the sum includes all non redundant pairs and ϵ_{ab} is the energy by each pair; the three-body term is

$$E_3(abcd) = \sum_{a<b<c} \epsilon_{abc} = \sum_{a<b<c} [E(abc) - E_1(abc) - E_2(abc)] \quad (4)$$

where the sum includes all the unique trimers of the cluster and ϵ_{abc} is the energy by each triad; the four-body contribution of the tetramer is given by

$$E_4 = \epsilon_{abcd} = E(abcd) - E_1(abcd) - E_2(abcd) - E_3(abcd) \quad (5)$$

This decomposition of the interaction energy is suitable for gaining insight of the nature and strength of the "beyond-2-body energies", as was pointed out by Gillan.[21] For the purposes of this work, this type of decomposition is used to analyze the relevance of interactions that govern the stability of the L-cystine crystal including its cooperative effects. In addition, the analysis allows us to establish the magnitude and the repulsive and attractive characters of such cooperative effects. The decomposition was applied to total energies as well as to the dispersion corrections to figure out the impact of each kind of term in the interaction energy of representative structures of the crystal.

METHODOLOGY

The optimization of the lattice parameters and internal coordinates within the unit cell was carried out using the experimental crystal structure of L-cystine as starting point. For such optimization, the PAW[22,23] method with the PBE-TS[15,16] functional was used within the VASP[24−27] program; four k points, obtained from the Monkhorst−Pack method, and an energy cutoff of 800 eV were used. The construction of the clusters was carried out by using a 2 × 2 × 2 supercell, from which two representative tetramers of L-cystine were extracted (Figure 2). The calculation of the energy decomposition of the clusters was done according to eqs 1−5 with cubic supercells of 24 Å per side for cluster A, and 20 Å for cluster B; three methods were tested: PBE,[28,29] TS,[15] and MBD.[17] For this case, one k-point, norm-conserving pseudopotentials and 1000 eV of energy cutoff, within the CASTEP[30] program, were used.

RESULTS AND DISCUSSION

The optimization was carried out using the experimental unit cell[9] as starting point: $a = b = 5.27$ Å and $c = 53.55$ Å, with a volume value of 1286.15 Å^3. All the lattice parameters are overestimated by the functional PBE, a and b have a percentage error of 4%, c of 8%, and the volume of 17%. The functional PBE + TS also overestimates the values but fixes them in the proper direction: the percentage errors for a and b are 3%, for c 5%, and for the volume 11%. As we can see in Table 1, PBE-TS and PBE show a good performance to describe the most important covalent bonds. In relation to the intermolecular interactions, PBE overestimates the distances and PBE-TS corrects in the right direction. One may distinguish two different regimes: bifurcated hydrogen bonds, *ii* and *iii* (in Figures 2.1 and 2.3), and S···S moieties have the largest errors, with a maximum around 9% for the hydrogen bond with smaller N−H···O angle, *iii*; and the standard hydrogen bonds *iv* with a maximum error of around 2%.

Table 1. Comparison of Calculated Atom−Atom Distances with the Experimental Values in Angstroms[a]

bond	exp[9]	PBE-TS	PBE
S—S	2.04	2.03	2.04
S—C	1.82	1.82	1.82
C—O	1.27	1.28	1.28
C═O	1.24	1.26	1.26
C—C	1.54	1.54	1.55
C—N	1.48	1.49	1.49
S···S	3.26	3.46	3.53
^{i}N—H···O	2.79	2.82	2.85
^{ii}N—H···O	2.64	2.74	2.79
^{iii}N—H···O	2.97	3.23	3.28
^{iv}N—H···O	2.70	2.76	2.82

[a]The hydrogen-bond lengths, N−H···O, correspond to the donor−acceptor distances. There are four types of such interactions as exemplified in Figure 2: ^{i}N−H···O has an angle value of 152°, ^{ii}N−H···O of 166.7°, ^{iii}N−H···O of 130.1°, and ^{iv}N−H···O of 160.8°.

Many-Body Decomposition in Clusters of L-Cystine. To evaluate the energy decomposition of eqs 2−5 for clusters A and B (Figures 2.1 and 2.3, respectively), it is required to calculate interaction energies for all dimers and trimers within each cluster. The clusters were selected so that they contain representative interactions, involved in the stabilization of the crystal, as they were identified before.[9] In cluster A (Figure 2.1) the interactions are of head-to-tail type, which are present along the C axis and in the A−B plane; the tetramer has nine hydrogen bonds and one S···S interaction. The cluster B (Figure 2.2) was chosen to represent the ring type interactions present in the A−B plane; in this case, the tetramer has ten hydrogen bonds and two S···S interactions; a perpendicular view of this cluster, Figure 2.3, clearly shows a ring-shaped structure of hydrogen bonds. To give an idea of the structures involved in the energy decomposition of eqs 1−5, in Figure 3 and Figure 4 some examples of such structures are displayed. These cases exemplify the differences between the number and kind of interactions associated with dimers and trimers.

In Figure 5 the energy contributions, two-body, three-body, and four-body, obtained for cluster A (Figure 2.1 and Figure 3) are displayed. The dimers (ac) and (bd) exhibit a head-to-tail conformation because, for instance, the group COO^- of molecule a forms one hydrogen bond with the group NH_3^+ of molecule c; it is also possible to say that it is a head-to-head interaction, because the head of molecule a is interacting with the head of molecule c. Globally, this interaction involved two hydrogen bonds whose average interaction energy is around 19 kcal/mol; as can be concluded from Figures 3 and 5, the dimer (ab) has one hydrogen bond of a strength around 15 kcal/mol. The (cd) dimer has two bifurcated hydrogen-bond moieties that involve four hydrogen bonds. In addition, it has one S···S interaction, and consequently, this is the dimer with higher interaction energy. In contrast, (bc) and (ad) have only long-range repulsive interactions. The three-body energy contributions are repulsive in (abc), (bcd), and (acd), but attractive in (abd). It can also be seen that for this tetramer the four-body contribution is attractive. It is noteworthy that the PBE functional describes three-body and four-body contributions with a minimal difference with respect to dispersion-corrected methodologies. Considering the dispersion corrections, Figure

DOI: 10.1021/acs.jpca.6b03167
J. Phys. Chem. A 2016, 120, 4223−4230

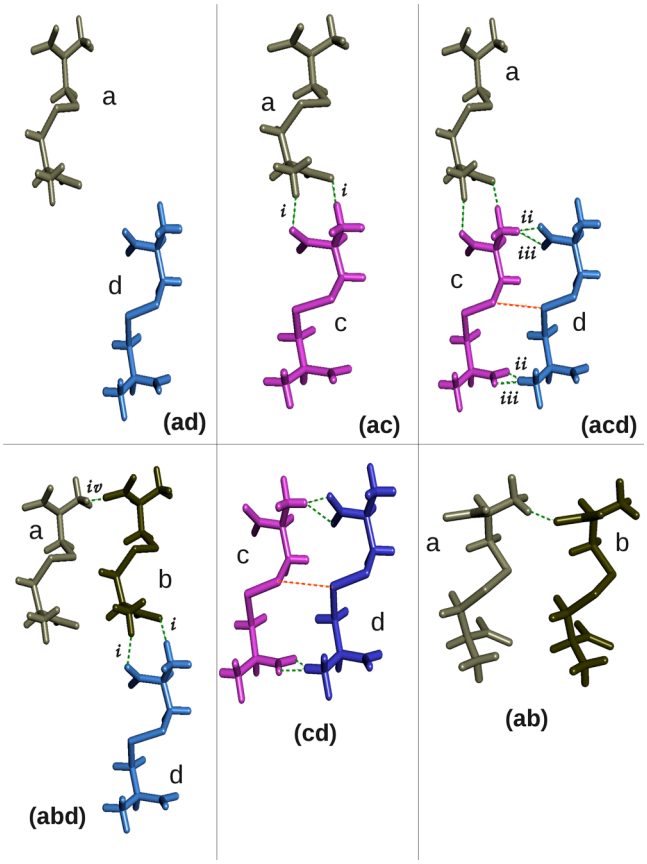

Figure 3. Schematic representation of some dimers and trimers of cluster A of Figure 2.1. The hydrogen-bond distances D−H···A are indicated in green. The S···S interactions are in orange. The four molecules of the tetramer are indicated as *a*, *b*, *c*, and *d*. The (*bc*) dimer is similar to (*ad*), and it has long-range interactions. The dimer (*ac*) is similar to (*bd*), and it has two hydrogen bonds. The dimer (*cd*) has four hydrogen bonds and one S···S interaction; the dimer (*ab*) has only one hydrogen bond. The trimer (*bcd*) is similar to (*acd*), and it has six hydrogen bonds and one S···S interaction. The trimer (*abd*) has three hydrogen bonds.

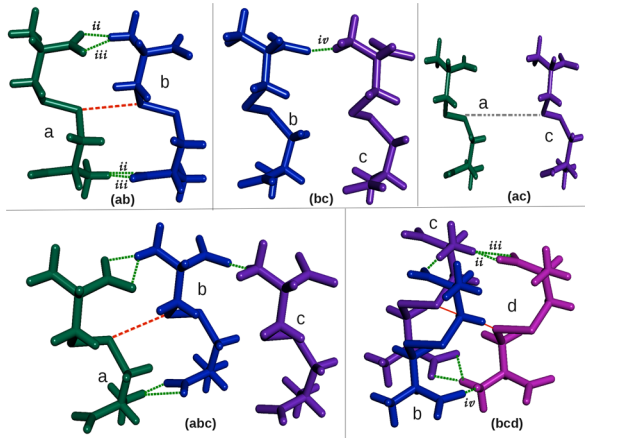

Figure 4. Schematic representation of some dimers and trimers of cluster B of Figure 2.2. The hydrogen-bond distances D−H···A are indicated as a green dotted line. The S···S interactions are in orange. The four molecules of the tetramer are indicated as *a*, *b*, *c*, and *d*. The (*ab*) dimer is similar to (*cd*), and it has four hydrogen bonds. The dimer (*bc*) has one hydrogen bond, and it is similar to (*ad*) and (*bd*). The dimer (*ac*) only has long-range interactions. The trimer (*abc*) has five hydrogen bonds and is equivalent to (*acd*). The trimer (*bcd*) has six hydrogen bonds and is equivalent to (*abd*). To obtain a better representation of the (*ac*) pair, the image had to be decreased due to the long distance between the molecules.

5b, the two-body terms evaluated by the MBD method are smaller than the ones calculated by the TS method; a situation that is completely different for the three-body and four-body terms in which the MBD values are clearly larger. Also, one may notice that the three-body dispersion contributions are all attractive and the four-body is repulsive, indicative of an oscillatory behavior in the many-body terms for these kind of structures in the solid. As was pointed out, the nature of attractive three-body terms corresponds to polarization-dispersion coupling,[18,31] and in this particular case they are not able to change the repulsive nature of the total three-body terms.

In Figure 6 the two-body, three-body, and four-body energy contributions, obtained for the ring-shape cluster B (Figure 2.2 and Figure 4) are displayed. At this point is important to mention that the identification of the structures in Figure 5 and Figure 6 are independent for each figure and in agreement with Figures 3 and 4, respectively; also, there are dimers that are equivalent in both structures. Accordingly, the dimer (*cd*) in Figure 5a is equivalent to the dimers (*ab*) and (*cd*) in Figure 6a; in addition, the dimer (*ab*) in Figure 5a is equivalent to dimers (*bc*), (*ad*), and (*bd*) of Figure 6a. Therefore, the only different kind of dimer in cluster B as compared to cluster A is the dimer (*ac*) in Figure 4 that has only long-range interactions; in contrast to the dimer (*ad*) of Figure 3, in this case the total interaction is attractive as well as the dispersive contribution. Thus, the dimers of kind (*ac*) in Figure 4 have an attractive contribution to the interaction energy whereas the ones of type (*ad*) in Figure 3 have a repulsive one. For tetramer B the three-body contribution is attractive in trimers (*abc*) and (*acd*), but quite repulsive in (*bcd*) and (*abd*). The four-body term in B is smaller than in A and it is repulsive. The dispersion contributions of the interaction energy in cluster B, Figure 6b, follow the same trends as in cluster A: the two-body terms evaluated by the MBD method are smaller than the ones evaluated with TS procedure, and the opposite situation is seen for the three- and four-body contributions. Again, the description of three-body and four-body terms by PBE is equivalent to the one obtained by the dispersion corrected methods. One point to notice is that in cluster B, the trimers (*bcd*) and (*abd*) have significant greater three-body attractive dispersion contributions but they are not enough to compensate the repulsive strong three-body nondispersive contributions giving rise to a global three-body term of around 10 kcal/mol; consequently, these kinds of trimers in the solid structure will contribute with three-body terms to destabilize the crystal. However, the dimeric contributions are stronger enough to fully compensate these repulsions and stabilize the crystal.

Strength of Different Interactions in the L-Cystine Crystal. To establish an approximate value for the S···S interaction energy between two molecules of L-cystine within the molecular crystal, we calculate the interaction energy of two L-cystine molecules whose geometry was extracted from the optimized crystal and the zwitterionic environment was substituted by methyl groups (Figure 2.4). The interaction energy is of the order of 3.5 kcal/mol (Table 2) regardless of the dispersion correction used; as the dispersion energy contribution is around 3 kcal/mol, one may say that this

DOI: 10.1021/acs.jpca.6b03167
J. Phys. Chem. A 2016, 120, 4223−4230

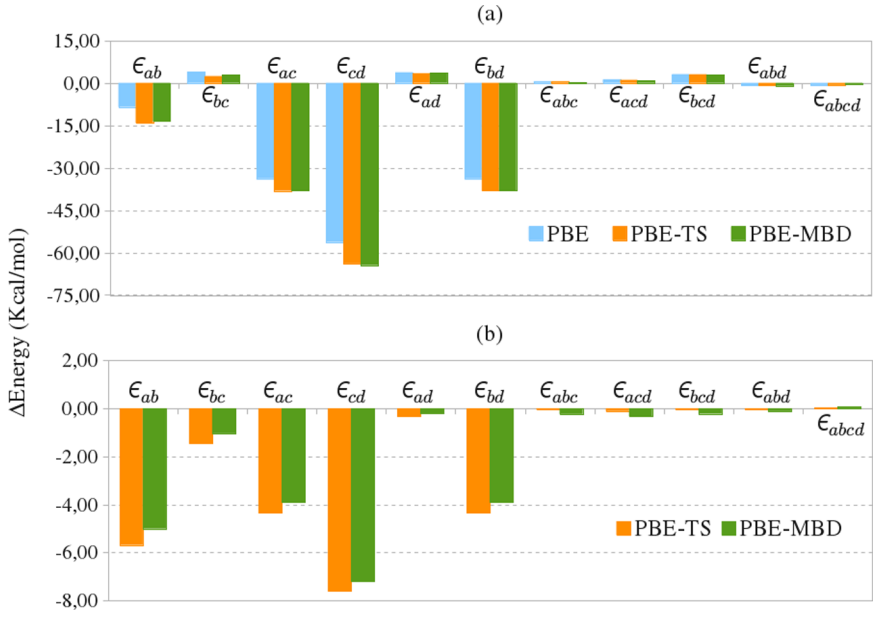

Figure 5. (a) Total interaction energy of each pair, triad, and tetramer involved in the cluster A (Figure 3). (b) Dispersion contributions to the interaction energy for each pair, triad, and tetramer. The color code is PBE in blue, PBE-TS in orange, and PBE-MBD in green.

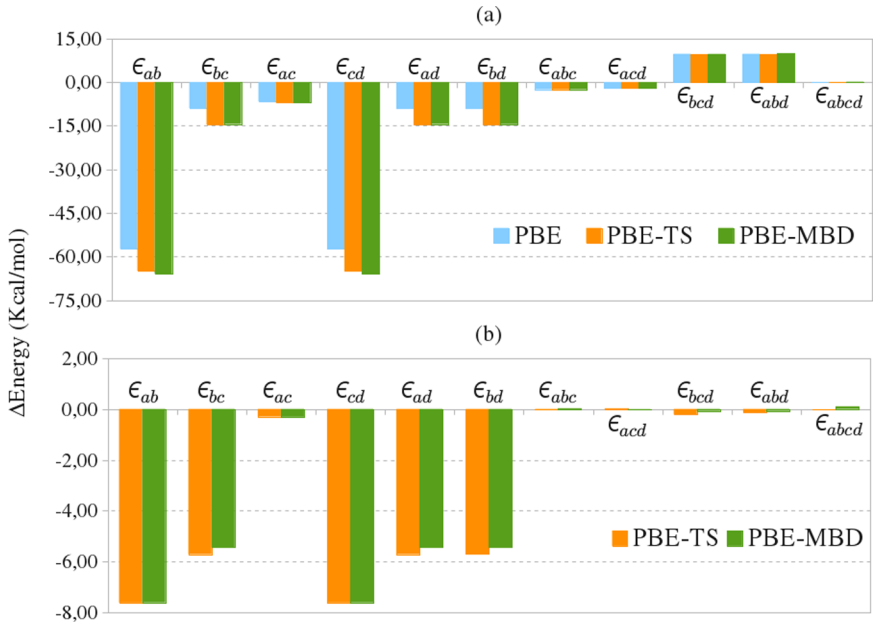

Figure 6. (a) Total interaction energy of each pair, triad, and tetramer involved in the cluster B of Figure 4. (b) Dispersion contributions to the interaction energy by each pair, triad, and tetramer. The color code is PBE in blue, PBE-TS in orange, and PBE-MBD in green.

Table 2. Interaction Energies Obtained with the PBE-MBD Method

type of interaction	interaction energy (kcal/mol)
[i]N−H···O	−19.02
[ii]N−H···O	∼−15.34[a]
[iii]N−H···O	∼−15.34
[iv]N−H···O	−13.57
S···S	−3.46[b]

[a]The ∼ symbol indicates that the value is an average estimation because the interaction energies [ii]N−H···O and [iii]N−H···O cannot be calculated independently. [b]This interaction energy was calculated from the modified L-cystine dimer (Figure 2.4).

interaction is mainly of van der Waals type. Our results go along with the study of Carme Rovira and Juan J. Novoa;[12] they performed a statistical analysis of the geometrical arrangement of the shortest S···S contacts found in neutral crystals of TTF-based molecules. In their study, most of the S···S contacts in the neutral crystals lie in the 3.4−4.3 Å range, with a maximum interaction energy at 3.93 Å; their *ab initio* MP2 data indicate that the S···S interactions for the interacting molecules analyzed by them can be as strong as 1.5 kcal/mol if the proper substituents are selected. In our case, for the dimer shown in Figure 2.4, the interaction value is significantly greater as calculated with PBE-MBD or PBE-TS methods.

The L-cystine molecule is a dipeptide linked by a disulfide bridge; this fact has some consequences in the zwitterionic

DOI: 10.1021/acs.jpca.6b03167
J. Phys. Chem. A 2016, 120, 4223−4230

hydrogen-bond networks formed in the crystal as compared to those in the dipeptide molecular solids in which the dipeptide is linked by a peptidic bond: (1) in the hexagonal crystal of L-cystine the head-to-head interaction along the C axis involves moieties with two hydrogen bonds, and these moieties are separated by a dipeptidic environment with the disulfide bridge in the middle (five bonds, two C—C, two C—H, and one S—S); (2) in the L-cystine crystal there are no hydrogen bonds associated with the −NH donor and −C═O acceptor of the peptidic bond. The regions containing double zwitterionic hydrogen bonds mentioned above are related to other key feature of the L-cystine crystal: the formation of layers of hydrogen-bond networks in the AB plane that resemble those formed in the glycine crystal.

In previous experimental and theoretical studies it has been determined that the planes $(10\bar{1}0)$ and $(\bar{1}010)$ have the lowest binding energies because they are related to the S···S interactions;[32,33] in contrast, the planes $(1\bar{1}00)$, $(\bar{1}100)$, $(0\bar{1}10)$, and $(01\bar{1}0)$ are related to the formation of the ring-shape networks containing hydrogen bonds of *ii*, *iii*, and *iv* types (Figure 2). These results are in agreement with the interaction energies displayed in Table 2.

In relation to the dislufide bridge environment it has been pointed out that S···S close contacts in the crystal also form a network along the A axis (see for instance Figure 3 of Moggach et al.[9]). By using the value of the S···S interaction obtained above and the interaction energies of the dimers in Figures 5a and 6a, one can estimate the interaction energy of each type of hydrogen bond. In Table 2 a summary of these estimated values is displayed; all energies were evaluated in the geometries obtained from the crystal structure. These values are obtained from molecule−molecule interactions and, consequently, represent estimations of the isolated interaction energies. The average of the interaction energy of hydrogen bonds is around 15 kcal/mol, the donor−acceptor distance is between 2.5 and 3 Å, and the angle value is bounded by 130° and 180°. According to the nature of the N−H···O interaction, we can say that the hydrogen bonds *iii* and *iv* are strong; however, the *i* type can be identified as very strong. A summary of the interactions associated with each L-cystine molecule within the crystal environment is displayed in Figure 7; in total, each molecule has the capability of forming ten hydrogen bonds and two S···S interactions.

The energy decomposition performed in this work supported the idea that the interaction networks formed in the L-cystine crystal are composed mainly of *strong* and *very-strong* hydrogen bonds, and also of S···S interactions. As in other peptide and dipeptide crystals, the strength of the hydrogen bonds present in this system is due to the zwitterionic nature of the molecule within the crystal. Although the L-cystine molecules contain net charges in the amine and carboxyl groups, our energy decomposition indicates that there are not strong Coulombic repulsions as has been determined in other systems such as the croconate crystals.[34] The repulsive three-body terms determined for the trimers (*bcd*) and (*abd*) of cluster B (Figure 4) and the trimer (*bcd*) of cluster A (Figure 3) are remarkable; these destabilizing contributions are of the order of 10 kcal/mol each in cluster B (Figure 6a) and of 3 kcal/mol for cluster A (Figure 5a). For all the trimers mentioned above, the three-body dispersion contribution is attractive and less than 0.5 kcal/mol. Let us analyze the interacting environments associated with the large three-body terms; to begin with, consider the trimer (*bcd*) in cluster B (Figure 4). Using the

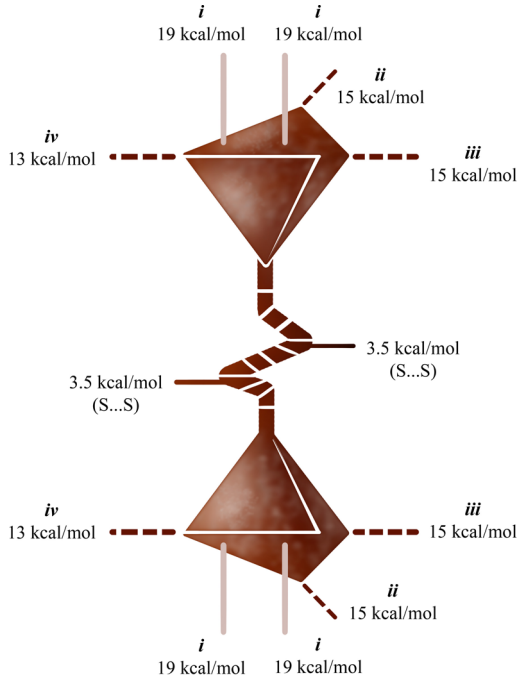

Figure 7. Schematic representation of the interaction pattern of the L-cystine molecule within its hexagonal crystal structure. The double head nature of the molecule is represented by the pyramid volumes, whereas the disulfide bridge motif corresponds to the sigmoid form in the center. The pale beige solid lines represent the strongest hydrogen bonds along the C axis, the broken lines represent the hydrogen bonds present in the AB plane, associated with the ring-shape structures found within the crystal, and the solid lines in the middle of the structure correspond to the S···S interactions. The nomenclature for hydrogen-bond types is according to Table 2.

schematic classification of Figure 7, one may say that the three-body contribution can be assigned to a moiety in which two heads are interacting in the AB plane through two hydrogen bonds (*ii* and *iii*) and the third head is interacting in the same plane but through an hydrogen bond of type *iv*; this situation corresponds to a nonadditive repulsive contribution of the order of 10 kcal/mol. In the case of the trimer (*acd*) in cluster A (Figure 3), the three-body term involves two heads interacting on the AB plane through hydrogen bonds of type *ii* and *iii* and one head interacting along the C axis with two hydrogen bonds of type *i* giving rise to a nonadditive repulsive term of the order of 3 kcal/mol. At this point one may try to rationalize the impact of an *imposter* molecule in the structure; these inhibitors are designed to have the same disulfide bridge environment as L-cystine but the hydrogen-bond-forming capabilities of the two "heads", of the molecule are partially cut out.[3,35] As one of these molecules occupies a place in the crystal, the rich connectivity of the heads of the molecule within the crystal is lost and the possibilities of the hydrogen-bond networks to keep growing are significantly reduced; in addition, the hydrogen bonds that could be formed by the intruder molecule are not so strong as the zwitterionic type formed by L-cystine; one has to keep in mind that zwitterionic hydrogen bonds are so strong that they are able to compensate nonadditive three-body terms of the order of a medium strength hydrogen bond (10 kcal/mol). In addition to the disruption of the hydrogen-bond networks, a more intriguing effect in which the *imposter* molecule[32] creates stoppers that inhibit the growing process of the (0001) layer has been

DOI: 10.1021/acs.jpca.6b03167
J. Phys. Chem. A 2016, 120, 4223−4230

determined;[33] the experiments also show that L-CDME is preferably incorporated so that the S−S bond is parallel to the edge of the step, which is along the direction in which the networks of S···S interactions are formed. Our results indicate that, in the crystal moiety, the S···S interaction is stronger than equivalent interactions between small molecules. This strong interaction supports the fact that the S···S motif has a key role in the attachment of L-CDME. The networks of hydrogen bonds on the plane AB are quite rigid, as has been determined by studying the crystal under pressure[9] in analogy to the results obtained for glycine.[10] In addition, the flexibility observed along the C axis in L-cystine crystal is related to the fact that the S···S interactions network is of van der Waals nature and indicates that the strongest hydrogen bonds in the structure, type *i*, only contribute to tighten the head-to-head interaction without any impact to rigidize the structure in that direction.

CONCLUSIONS

The zwitterionic nature of the L-cystine molecules in the crystal gives rise to strong hydrogen bonds that are related to the remarkable stability of this crystal. Also, from the energy decomposition performed in this work, a picture of the interaction capabilities of each L-cystine molecule within the crystal structure emerges; this interaction pattern, summarized in Figure 7, provides a clear differentiation of the strengths of the different interactions within the crystal. Using this interaction pattern, one may visualize the structure of the crystal as composed of planes of head-to-head sites, each of them stabilized by two of the strongest hydrogen bonds formed in the crystal (19 kcal/mol); the network of head-to-head sites, residing in the AB plane, is a rigid structure because each site has the possibility of forming two hydrogen bonds of around 15 kcal/mol and one of 13 kcal/mol. Such networks are related to the high binding energies in the planes $(1\bar{1}00)$, $(\bar{1}100)$, $(0\bar{1}10)$, and $(01\bar{1}0)$ of the hexagonal crystal structure. Between two consecutive head-to-head planes along the C axis, one has a network of S···S interactions (3.5 kcal/mol) that are mainly of van der Waals type; they are related to the low binding energies in the planes $(10\bar{1}0)$ and $(\bar{1}010)$, as well as to the flexibility of the crystal along the C axis. There are some structural features in the crystal that induce repulsive three-body contributions of the order of magnitude of a hydrogen bond (approximately 10 kcal/mol); these repulsive contributions coexist with smaller attractive three-body nonadditive dispersion terms. The ring-shape conformations shows the biggest dispersion contribution to the interaction energy. There are important dispersion contributions to the hydrogen-bond interaction in representative structures of the crystal. Four-body contributions are quite small, and only the MBD method is able to give significant values of such contributions. The many-body decomposition used in this work is an appropriate tool to examine the attractive and repulsive nature of the three- and four-body contributions to the total interaction energy. Along this vein, it is worthwhile to mention that the cohesive energy per molecule evaluated using the MBD method is around 90 kcal/mol; if one compares this value with a rough estimation of the interaction energy using a pairwise approach coming from the data of Figure 7, which is around 97.5 kcal/mol, one may see that this difference is congruent with the fact that the biggest many-body contributions evaluated in this work are the repulsive three-body terms. Also, the energy decomposition performed in this work indicates that, for this system, PBE gives a reasonable description of the three- and four-body terms. Finally, it is determined without doubt that the interaction energy between S···S is of van der Waals type.

AUTHOR INFORMATION

Corresponding Author

*M. Galván. E-mail: mgalvan@xanum.uam.mx. Phone: 00-52-5558044600, ext 3277.

Notes

The authors declare no competing financial interest.

ACKNOWLEDGMENTS

The authors thank Dr. Alfredo Guevara and Dr. Anthony Reilly for many helpful discussions; and to the referees for their enriching and positive comments. We also thank LSVP laboratory at UAM-I and FHI-Theory Department for giving us access to their computer facilities and to E. Galván for figure design. A.F.G.H. gratefully acknowledges CONACYT for a Ph.D. scholarship. This work was supported in part by CONACYT grants 155698 and 154784.

ABBREVIATIONS

DFT, density-functional theory; GGA, generalized-gradient approximation; MBD, many-body dispersion; L-CDME, L-cystine dimethyl ester; PAW, projected augmented wave method

REFERENCES

(1) Thoene, J. G. Cystinosis. *J. Inherited Metab. Dis.* **1995**, *18*, 380−386.
(2) Gahl, W. A.; Thoene, J. G.; Schneider, J. A. Cystinosis. *N. Engl. J. Med.* **2002**, *347*, 111−121.
(3) Rimer, J. D.; An, Z.; Zhu, Z.; Lee, M. H.; Goldfarb, D. S.; Wesson, J. A.; Ward, M. D. Crystal Growth Inhibitors for the Prevention of L-Cystine Kidney Stones Through Molecular Design. *Science* **2010**, *330*, 337−341.
(4) Oughton, B. M.; Harrison, P. M. The Crystal Structure of Hexagonal L-Cystine. *Acta Crystallogr.* **1959**, *12*, 396−404.
(5) Dahaoui, A.; Pichon-Pesme, V.; Howard, J. A. K.; Lecomte, C. CCD Charge Density Study on Crystals with Large Unit Cell Parameters: The Case of Hexagonal L-Cystine. *J. Phys. Chem. A* **1999**, *103*, 6240−6250.
(6) Roux, M. V.; Foces-Foces, C.; Notario, R.; Ribeiro da Silva, M. A. V.; Ribeiro da Silva, M. d. D. M. C.; Santos, A. F. L. O. M.; Juaristi, E. Experimental and Computational Thermochemical Study of Sulfur-Containing Amino Acids: L-Cysteine, L-Cystine, and L-Cysteine-Derived Radicals. S-S, S-H, and C-S Bond Dissociation Enthalpies. *J. Phys. Chem. B* **2010**, *114*, 10530−10540.
(7) Kapustin, E. A.; Minkov, V. S.; Stare, J.; Boldyreva, E. V. One Hydrogen Bond−Two Ways To Build a Structure. The Role of N-H···O Hydrogen Bonds in Crystal Structures of N,N-Dimethylglycine. *Cryst. Growth Des.* **2014**, *14*, 1851−1864.
(8) Görbitz, C. H. Structures of Dipeptides: The Head-To-Tail Story. *Acta Crystallogr., Sect. B: Struct. Sci.* **2010**, *B66*, 84−93.
(9) Moggach, S. A.; Allan, D. R.; Parsons, S.; Sawyerb, L.; Warren, J. E. The Effect of Pressure on the Crystal Structure of Hexagonal L-Cystine. *J. Synchrotron Radiat.* **2005**, *12*, 598−607.
(10) Azuri, I.; Meirzadeh, E.; Ehre, D.; Cohen, S. R.; Rappe, A. M.; Lahav, M.; Lubomirsky, I.; Kronik, L. Unusually Large Youngs Moduli of Amino Acid Molecular Crystals. *Angew. Chem., Int. Ed.* **2015**, *54*, 13566−13570.
(11) Kolesov, B. A.; Boldyreva, E. V. Self-Trapped N-H Vibrational States in the Polymorphs of Glycine, L- and DL-Alanine. *J. Raman Spectrosc.* **2010**, *41*, 670−677.
(12) Rovira, C.; Novoa, J. J. Strength and Directionality of the S···S Intermolecular Interactions Present in TTF-Based Molecular Crystals.

DOI: 10.1021/acs.jpca.6b03167
J. Phys. Chem. A 2016, 120, 4223−4230

A Combined Statistical and Ab Initio Study. *Chem. - Eur. J.* **1999**, *5*, 3689−3697.
(13) Risthaus, T.; Grimme, S. Benchmarking of London Dispersion-Accounting Density Functional Theory Methods on Very Large Molecular Complexes. *J. Chem. Theory Comput.* **2013**, *9*, 1580−1591.
(14) Reilly, A.; Tkatchenko, A. Seamless and Accurate Modeling of Organic Molecular Materials. *J. Phys. Chem. Lett.* **2013**, *4*, 1028−1033.
(15) Tkatchenko, A.; Scheffler, M. Accurate Molecular van Der Waals Interactions from Ground-State Electron Density and Free-Atom Reference Data. *Phys. Rev. Lett.* **2009**, *102*, 073005.
(16) Bučko, T.; Lebègue, S.; Hafner, J.; Ángyán, J. G. Tkatchenko-Scheffler van Der Waals Correction Method with and without Self-Consistent Screening Applied to Solids. *Phys. Rev. B: Condens. Matter Mater. Phys.* **2013**, *87*, 064110.
(17) Ambrosetti, A.; Reilly, A. M.; DiStasio, R. A., Jr.; Tkatchenko, A. Long-Range Correlation Energy Calculated from Coupled Atomic Response Functions. *J. Chem. Phys.* **2014**, *140*, 18A508.
(18) Reilly, A. M.; Tkatchenko, A. van Der Waals Dispersion Interactions in Molecular Materials: Beyond Pairwise Additivity. *Chem. Sci.* **2015**, *6*, 3289−3301.
(19) Marom, N.; DiStasio, R. A., Jr.; Atalla, V.; Levchenko, S.; Reilly, A. M.; Chelikowsky, J. R.; Leiserowitz, L.; Tkatchenko, A. Many-Body Dispersion Interactions in Molecular Crystal Polymorphism. *Angew. Chem., Int. Ed.* **2013**, *52*, 6629−6632.
(20) Kaplan, I. G. *Intermolecular Interactions: Physical Picture,Computational Methods and Model Potentials*; Wiley: New York, 2006.
(21) Gillan, M. J. Many-Body Exchange-Overlap Interactions in Rare Gases and Water. *J. Chem. Phys.* **2014**, *141*, 224106.
(22) Blöchl, P. E. Projector Augmented-Wave Method. *Phys. Rev. B: Condens. Matter Mater. Phys.* **1994**, *50*, 17953−17979.
(23) Kresse, G.; Joubert, D. From Ultrasoft Pseudopotentials to the Projector Augmented-Wave Method. *Phys. Rev. B: Condens. Matter Mater. Phys.* **1999**, *59*, 1758−1775.
(24) Kresse, G.; Hafner, J. Ab Initio Molecular Dynamics for Liquid Metals. *Phys. Rev. B: Condens. Matter Mater. Phys.* **1993**, *47*, 558−561.
(25) Kresse, G.; Hafner, J. Ab Initio Molecular-Dynamics Simulation of the Liquid-Metal-Amorphous-Semiconductor Transition in Germanium. *Phys. Rev. B: Condens. Matter Mater. Phys.* **1994**, *49*, 14251−14269.
(26) Kresse, G.; Furthmüller, J. Efficiency of Ab-Initio Total Energy Calculations for Metals and Semiconductors Using a Plane-Wave Basis Set. *Comput. Mater. Sci.* **1996**, *6*, 15−50.
(27) Kresse, G.; Furthmüller, J. Efficient Iterative Schemes for Ab Initio Total-Energy Calculations Using a Plane-Wave Basis Set. *Phys. Rev. B: Condens. Matter Mater. Phys.* **1996**, *54*, 11169−11186.
(28) Perdew, J. P.; Burke, K.; Ernzerhof, M. Generalized Gradient Approximation Made Simple. *Phys. Rev. Lett.* **1996**, *77*, 3865−3868.
(29) Perdew, J. P.; Burke, K.; Ernzerhof, M. Erratum: Generalized Gradient Approximation Made Simple. *Phys. Rev. Lett.* **1997**, *78*, 1396.
(30) Clark, S. J.; Segall, M. D.; Pickard, C. J.; Hasnip, P. J.; Probert, M. I. J.; Refson, K.; Payne, M. C. First Principles Methods Using CASTEP. *Z. Kristallogr. - Cryst. Mater.* **2005**, *220*, 567−570.
(31) Tkatchenko, A.; Alfé, D.; Kim, K. S. First-Principles Modeling of Non-Covalent Interactions in Supramolecular Systems: The Role of Many-Body Effects. *J. Chem. Theory Comput.* **2012**, *8*, 4317−4322.
(32) Shtukenberg, A. G.; Zhu, Z.; An, Z.; Bhandari, M.; Song, P.; Kahr, B.; Ward, M. D. Illysory Spirals and Loops in Crystal Growth. *Proc. Natl. Acad. Sci. U. S. A.* **2013**, *110*, 17195−17198.
(33) Shtukenberg, A. G.; Poloni, L. N.; Zhu, Z.; An, Z.; Bhandari, M.; Song, P.; Rohl, A. L.; Kahr, B.; Ward, M. D. Dislocation-Actuated Growth and Inhibition of Hexagonal L-Cystine Crystallization at the Molecular Level. *Cryst. Growth Des.* **2015**, *15*, 921−934.
(34) Dunitz, J. D.; Gavezzotti, A.; Rizzato, S. Coulombic Compression, a Pervasive Force in Ionic Solids. A Study of Anion Stacking in Croconate Salts. *Cryst. Growth Des.* **2014**, *14*, 357−366.
(35) Mandal, T.; Ward, M. D. Determination of Specific Binding Interactions at L-Cystine Crystal Surfaces with Chemical Force Microscopy. *J. Am. Chem. Soc.* **2013**, *135*, 5525−5528.

DOI: 10.1021/acs.jpca.6b03167
J. Phys. Chem. A 2016, 120, 4223−4230